The Astrophysical Journal Letters, 921:L6 (8pp), 2021 November 1 https://doi.org/10.3847/2041-8213/ac2e90
© 2021 The Author(s). Published by the American Astronomical Society.
OPEN ACCESS

# Faintest of Them All: ZTF 21aaoryiz/SN 2021fcg—Discovery of an Extremely Low Luminosity Type Iax Supernova

Viraj R. Karambelkar[1], Mansi M. Kasliwal[1], Kate Maguire[2], Shreya G. Anand[1], Igor Andreoni[1], Kishalay De[1], Andrew Drake[1], Dmitry A. Duev[3], Matthew J. Graham[1], Erik C. Kool[4], Russ R. Laher[5], Mark R. Magee[2], Ashish A. Mahabal[3,6], Michael S. Medford[7,8], Daniel Perley[9], Mickael Rigault[10], Ben Rusholme[5], Steve Schulze[11], Yashvi Sharma[1], Jesper Sollerman[4], Anastasios Tzanidakis[1], Richard Walters[12], and Yuhan Yao[1]
[1] Cahill Center for Astrophysics, California Institute of Technology, Pasadena, CA 91125, USA; viraj@astro.caltech.edu
[2] School of Physics, Trinity College Dublin, the University of Dublin, College Green, Dublin, Ireland
[3] Division of Physics, Mathematics and Astronomy, California Institute of Technology, Pasadena, CA 91125, USA
[4] The Oskar Klein Centre, Department of Astronomy, Stockholm University, AlbaNova, SE-10691, Stockholm, Sweden
[5] IPAC, California Institute of Technology, 1200 E. California Boulevard, Pasadena, CA 91125, USA
[6] Center for Data Driven Discovery, California Institute of Technology, Pasadena, CA 91125, USA
[7] Department of Astronomy, University of California, Berkeley, Berkeley, CA 94720, USA
[8] Lawrence Berkeley National Laboratory, 1 Cyclotron Road, Berkeley, CA 94720, USA
[9] Astrophysics Research Institute, Liverpool John Moores University, 146 Brownlow Hill, Liverpool, L3 5RF, UK
[10] Univ Lyon, Univ Claude Bernard Lyon 1, CNRS, IP2I Lyon/IN2P3, IMR 5822, F-69622, Villeurbanne, France
[11] The Oskar Klein Centre, Department of Physics, Stockholm University, AlbaNova, SE-10691, Stockholm, Sweden
[12] Caltech Optical Observatories, Pasadena, CA 91125, USA
*Received 2021 August 13; revised 2021 October 7; accepted 2021 October 7; published 2021 October 27*

## Abstract

We present the discovery of ZTF 21aaoryiz/SN 2021fcg—an extremely low luminosity Type Iax supernova. SN 2021fcg was discovered by the Zwicky Transient Facility in the star-forming galaxy IC0512 at a distance of ≈27 Mpc. It reached a peak absolute magnitude of $M_r = -12.66 \pm 0.20$ mag, making it the least luminous thermonuclear supernova discovered to date. The $E(B-V)$ contribution from the underlying host galaxy is unconstrained. However, even if it were as large as 0.5 mag, the peak absolute magnitude would be $M_r = -13.78 \pm 0.20$ mag—still consistent with being the lowest-luminosity SN. Optical spectra of SN 2021fcg taken at 37 and 65 days post-maximum show strong [Ca II], Ca II, and Na I D emission and several weak [Fe II] emission lines. The [Ca II] emission in the two spectra has extremely low velocities of ≈1300 and 1000 km s$^{-1}$, respectively. The spectra very closely resemble those of the very low luminosity Type Iax supernovae SN 2008 ha, SN 2010ae, and SN 2019gsc taken at similar phases. The peak bolometric luminosity of SN 2021fcg is $\approx 2.5^{+1.5}_{-0.3} \times 10^{40}$ erg s$^{-1}$, which is a factor of 3 lower than that for SN 2008 ha. The bolometric lightcurve of SN 2021fcg is consistent with a very low ejected nickel mass ($M_{\rm Ni} \approx 0.8^{+0.4}_{-0.5} \times 10^{-3}\ M_\odot$). The low luminosity and nickel mass of SN 2021fcg pose a challenge to the picture that low-luminosity SNe Iax originate from deflagrations of near-$M_{\rm ch}$ hybrid carbon–oxygen–neon white dwarfs. Instead, the merger of a carbon–oxygen and oxygen–neon white dwarf is a promising model to explain SN 2021fcg.

*Unified Astronomy Thesaurus concepts:* Type Ia supernovae (1728); White dwarf stars (1799); Time domain astronomy (2109)

*Supporting material:* data behind figures

## 1. Introduction

Type Iax supernovae (SNe) are a peculiar subclass of Type Ia SNe (Foley et al. 2013). These events are named after the prototypical SN 2002cx (Li et al. 2003) and are characterized by slower expansion speeds (2000–8000 km s$^{-1}$) and a diverse range of luminosities compared to normal SNe Ia (Jha 2017). The luminosities of SNe Iax vary from $M_r \approx -19$ at the bright end (SN 2008A; McCully et al. 2014) to $M_r \approx -14$ at the faint end (SN 2008 ha; Foley et al. 2009; Valenti et al. 2009). SNe Iax account for ∼31% of the total SN Ia rate (Foley et al. 2013) and are believed to be associated with thermonuclear explosions of white dwarfs (Jha 2017). However, their exact progenitors and explosion mechanisms still remain unknown.

Original content from this work may be used under the terms of the Creative Commons Attribution 4.0 licence. Any further distribution of this work must maintain attribution to the author(s) and the title of the work, journal citation and DOI.

Four SNe Iax have been discovered with very low luminosities ($M_V \approx -14$) and explosion energies—SN 2008 ha ($M_V = -14.2$; Foley et al. 2009; Valenti et al. 2009), SN 2010ae ($-13.8 > M_V > -15.3$; Stritzinger et al. 2014), SN 2019gsc ($M_r = -13.9$; Srivastav et al. 2020; Tomasella et al. 2020), and SN 2019ttf ($M_r \approx -14$; De et al. 2020), although only the first three have been studied extensively. These SNe have low ejected nickel masses ($\sim 10^{-3}\ M_\odot$) and a faster evolution than their brighter counterparts. Several explosion mechanisms have been proposed to account for the low luminosities and nickel masses of faint SNe Iax—partial deflagration of a hybrid CONe white dwarf (Kromer et al. 2015), merger of a CO and ONe white dwarf (Kashyap et al. 2018), a helium nova (McCully et al. 2014), an ultra-stripped electron-capture SN (Pumo et al. 2009), and a "fallback" massive star SN (Moriya et al. 2010). However, the small sample of these events makes it difficult to distinguish between these models.

In this Letter, we present the discovery of ZTF 21aaoryiz or SN 2021fcg—the least luminous member of the SN Iax class. SN 2021fcg has a peak $M_r = -12.66 \pm 0.20$ and is the

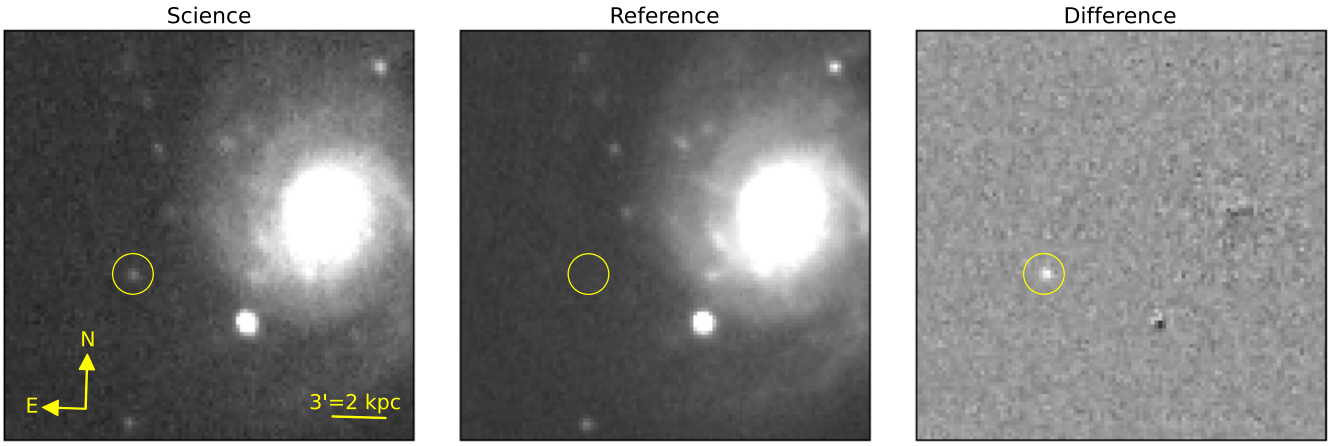


**Figure 1.** ZTF *r*-band science, reference, and difference discovery images of SN 2021fcg. The position of the supernova is marked with a yellow circle. The science image was taken on MJD 59,281.22.

lowest-luminosity thermonuclear SN discovered to date. Here, we present optical photometric and spectroscopic follow-up of this transient. In Section 2, we describe the discovery and details of our follow-up observations. In Section 3 we analyze the lightcurve to derive ejecta masses. In Section 4, we present the spectroscopic evolution of this SN. In Section 5, we discuss this SN in the context of different formation scenarios. We conclude with a summary of our results in Section 6.

## 2. Discovery and Follow-up Observations

### 2.1. Discovery

SN 2021fcg was discovered by the Zwicky Transient Facility (ZTF; Bellm et al. 2019; Graham et al. 2019; Dekany et al. 2020), which runs on the Palomar 48 inch (P48) Oschin Schmidt telescope. The first real-time alert (Patterson et al. 2019) was generated on 20210308.22 UT (MJD 59,281.22) at J2000 coordinates of $\alpha = 09^{h}04^{m}32\overset{s}{.}37$, $\delta = +85^{d}29^{m}48\overset{s}{.}44$. The transient was automatically tagged as a supernova candidate by a machine-learning-based Alert-Classifying Artificial Intelligence program (D. A. Duev et al. 2021, in preparation). It was later flagged by the Census of Local Universe program (see De et al. 2020 for details) that identifies transients associated with nearby (<200 Mpc) galaxies on the Fritz portal (Duev et al. 2019; Kasliwal et al. 2019; van der Walt et al. 2019). Figure 1 shows the ZTF discovery image of this transient.

### 2.2. Host Galaxy and Extinction

SN 2021fcg is located on the outskirts of the star-forming spiral galaxy IC0512 at a physical separation of ≈7.5 kpc (angular separation ≈53″) from the nucleus (Figure 1). The host galaxy has a redshift of $z = 0.005384$ and a heliocentric velocity of $1614 \pm 10\,\mathrm{km\,s^{-1}}$ (Kourkchi & Tully 2017). Correcting for the Virgo Infall, Shapley cluster, and Great Attractor (Mould et al. 2000) gives a distance modulus $\mu = 32.14 \pm 0.15$ mag (we use $H_0 = 73\,\mathrm{km\,s^{-1}\ Mpc^{-1}}$ in this Letter).[13]

The Galactic extinction along the line of sight to this galaxy is $A_V = 0.208$ mag (Schlafly & Finkbeiner 2011), for a standard reddening law with $R_V = 3.1$. We cannot estimate extinction due to the host galaxy accurately as our spectra do not show any absorption lines from the host. However, the supernova is located in the outskirts of the host galaxy where the host extinction is likely low (Figure 1). We thus adopt $E(B-V)_{\mathrm{tot}} = E(B-V)_{\mathrm{MW}} = 0.068$ mag. We discuss the implications of host extinction on our absolute magnitude estimates in Section 3.

### 2.3. Follow-up Observations

The field containing SN 2021fcg was observed on several epochs by the ZTF camera on P48 in the *g*, *r*, and *i* bands. The images were processed by the ZTF Data System Pipelines (Masci et al. 2019), which perform image subtraction based on the ZOGY algorithm (Zackay et al. 2016). We performed forced point-spread function photometry at the location of the transient in all subtracted ZTF images. We obtained additional *g*, *r*, and *i* band photometric observations with the Spectral Energy Distribution Machine (SEDM; Blagorodnova et al. 2018; Rigault et al. 2019) mounted on the 60 inch telescope at Palomar (P60) on MJD 59,306 and 59,318. We also observed the field in the *r* band with the Alhambra Faint Object Spectrograph and Camera (ALFOSC) at the 2.56 m Nordic Optical Telescope (Spain) on MJD 59,367. We reduced the data with the PyNOT[14] pipeline. Finally, the field was also observed by the ATLAS survey (Tonry et al. 2018; Smith et al. 2020). We used the ATLAS forced photometry service[15] to query all photometric measurements at the location of SN 2021fcg. We combined measurements from same-day observations by taking a weighted mean of the flux using the inverse of the square of the flux uncertainties as weights. All photometric measurements ($3\sigma$ detections and $5\sigma$ upper limits) are listed in Table 1.

Our spectroscopic follow-up comprises two optical spectra obtained with the Low Resolution Imaging Spectrograph (LRIS; Oke et al. 1995) on the Keck I 10 m telescope. The spectra were obtained on MJD 59,318 and 59,344 corresponding to +37 days and +63 days after the *r*-band maximum of SN 2021fcg. The spectra were reduced using the IDL-based tool `lpipe` (Perley 2019).

[13] Theureau et al. (2007) report a Tully–Fisher distance modulus of $31.82 \pm 0.41$ mag using $H_0 = 57\,\mathrm{km\,s^{-1}}$. Adopting $H_0 = 73\,\mathrm{km\,s^{-1}\ Mpc^{-1}}$ will reduce this distance modulus, making SN 2021fcg even lower luminosity than reported here.

[14] https://github.com/jkrogager/PyNOT

[15] https://fallingstar.com

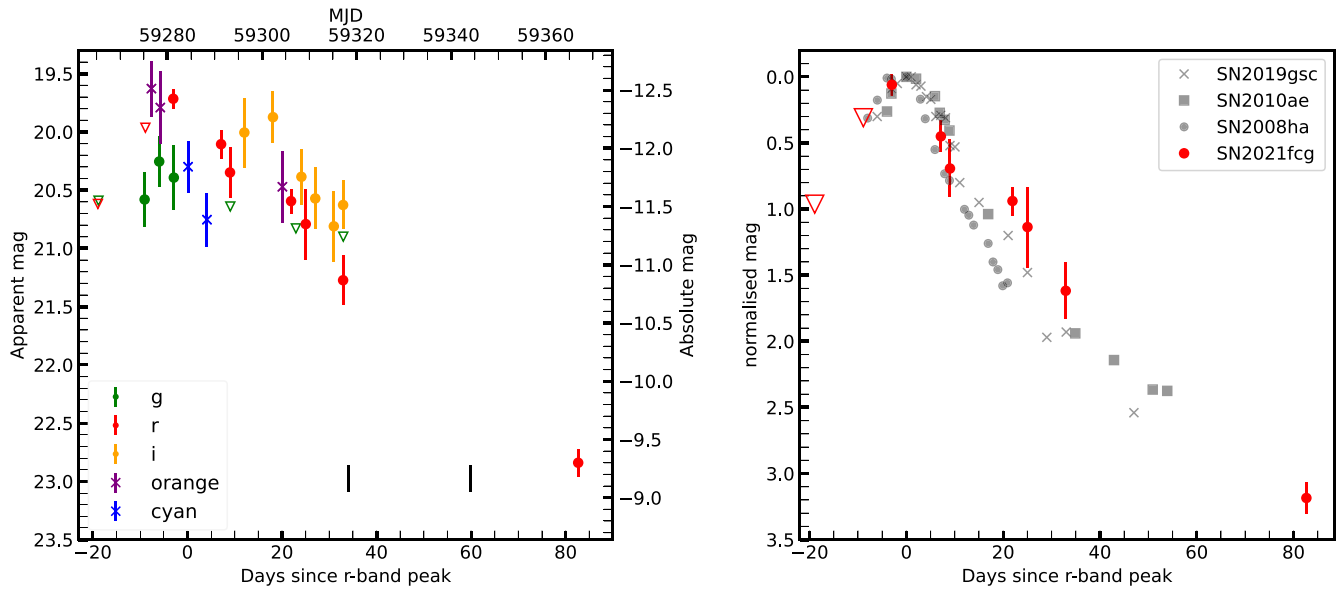


**Figure 2.** Left: *g*-, *r*-, *i*-, *o*-, and *c*-band lightcurve of SN 2021fcg. The epochs of our spectroscopic observations are marked with a black vertical line. Right: comparison of the *r*-band photometric evolution to other low-luminosity SN Iax (SNe 2008 ha, 2019gsc, and 2010ae). In the first 12 days post-maximum, the evolution of SN 2021fcg is similar to SNe 2010ae and 2019gsc, but slower than SN 2008 ha. After 12 days, the evolution of SN 2021fcg slows down, with a possible plateau between 12 and 22 days. This plateau is also seen in the *i*-band measurements (left panel). Data for the comparison objects are taken from Valenti et al. (2009), Stritzinger et al. (2015), and Srivastav et al. (2020), respectively. The lightcurve photometry of SN 2021fcg is available as the data behind the figure.

(The data used to create this figure are available.)

**Table 1**
Photometric Measurements of SN 2021fcg (>3$\sigma$ Detections and 5$\sigma$ Limits)

| MJD | Phase[a] | *g* | *r* | *i* | *c* | *o* | Instrument |
|---|---|---|---|---|---|---|---|
| 59,256.25 | −27.7 | >20.77 | >20.90 | ⋯ | ⋯ | ⋯ | ZTF |
| 59,265.28 | −18.7 | >20.59 | >20.62 | ⋯ | ⋯ | | ZTF |
| 59,270.45 | −13.5 | ⋯ | ⋯ | ⋯ | ⋯ | >19.27 | ATLAS |
| 59,275.16 | −08.8 | 20.58 ± 0.23 | >19.96 | ⋯ | ⋯ | ⋯ | ZTF |
| 59,276.61 | −07.4 | ⋯ | ⋯ | ⋯ | ⋯ | 19.63 ± 0.24 | ATLAS |
| 59,278.25 | −05.7 | 20.25 ± 0.22 | ⋯ | ⋯ | ⋯ | ⋯ | ZTF |
| 59,278.49 | −05.5 | ⋯ | ⋯ | ⋯ | ⋯ | 19.79 ± 0.31 | ATLAS |
| 59,281.22 | −02.8 | 20.39 ± 0.28 | 19.72 ± 0.08 | ⋯ | ⋯ | ⋯ | ZTF |
| 59,284.36 | +00.4 | ⋯ | ⋯ | ⋯ | 20.30 ± 0.22 | ⋯ | ATLAS |
| 59,288.35 | +04.3 | ⋯ | ⋯ | ⋯ | 20.75 ± 0.23 | ⋯ | ATLAS |
| 59,291.34 | +07.3 | ⋯ | 20.10 ± 0.12 | ⋯ | ⋯ | ⋯ | ZTF |
| 59,293.23 | +09.2 | >20.64 | 20.35 ± 0.22 | ⋯ | ⋯ | ⋯ | ZTF |
| 59,296.26 | +12.3 | ⋯ | ⋯ | 20.01 ± 0.30 | ⋯ | ⋯ | ZTF |
| 59,302.31 | +18.3 | ⋯ | ⋯ | 19.87 ± 0.22 | ⋯ | ⋯ | ZTF |
| 59,304.32 | +20.3 | | | | | 20.47 ± 0.31 | ATLAS |
| 59,306.14 | +22.1 | ⋯ | 20.59 ± 0.11 | ⋯ | ⋯ | ⋯ | SEDM |
| 59,307.16 | +23.2 | >20.83 | ⋯ | ⋯ | ⋯ | ⋯ | ZTF |
| 59,308.32 | +24.3 | ⋯ | ⋯ | 20.39 ± 0.24 | ⋯ | ⋯ | ZTF |
| 59,309.24 | +25.2 | ⋯ | 20.79 ± 0.30 | ⋯ | ⋯ | ⋯ | ZTF |
| 59,311.26 | +27.3 | ⋯ | ⋯ | 20.57 ± 0.27 | ⋯ | ⋯ | ZTF |
| 59,315.18 | +31.2 | ⋯ | ⋯ | 20.81 ± 0.30 | ⋯ | | ZTF |
| 59,317.65 | +33.7 | ⋯ | 21.27 ± 0.21 | 20.63 ± 0.21 | ⋯ | ⋯ | SEDM |
| 59,366.88 | +82.9 | ⋯ | 22.84 ± 0.12 | ⋯ | ⋯ | ⋯ | NOT |

**Note.**
[a] Phase is given in days since *r*-band peak.

## 3. Lightcurve Analysis

Figure 2 shows the lightcurve of SN 2021fcg.

We constrain the explosion time between MJD 59, 265.28 < $t_{exp}$ < 59, 275.16 (based on the latest, deepest nondetection and the first detection). The *g*-band lightcurve of SN 2021fcg has only three points that do not show significant evolution and hence samples the supernova around the peak. We report the mean of the three detections as the peak *g*-band magnitude. We also report the mean of the first two *o*-band detections as the peak *o* magnitude; however, this is poorly constrained as the latest *o* upper limit prior to first detection is

shallower than the first detection. We cannot constrain the *c*-band peak from our two detections. To determine the peak brightness in the *r* band, we use the lightcurve of SN 2019gsc as a template and fit the stretched-scaled template to the observed lightcurve of SN 2021fcg.

The extinction-corrected peak apparent magnitudes of SN 2021fcg are $m_o^{\rm peak} = 19.54 \pm 0.28$, $m_g^{\rm peak} = 20.16 \pm 0.24$, and $m_r^{\rm peak} = 19.48 \pm 0.14$ on MJD $59{,}284.0 \pm 1.5$ days. This corresponds to $M_o^{\rm peak} = -12.60 \pm 0.32$, $M_g^{\rm peak} = -11.66 \pm 0.42$, and $M_r^{\rm peak} = -12.66 \pm 0.20$ mag. This makes SN 2021fcg the lowest-luminosity SN discovered to date. The faintest previously known SN Iax are SN 2019gsc ($M_{\rm g}^{\rm peak} = -13.58 \pm 0.15$, $M_r^{\rm peak} = -14.28 \pm 0.15$; Srivastav et al. 2020; Tomasella et al. 2020), SN 2010ae ($M_{\rm g}^{\rm peak} = -14.2 \pm 0.5$, $M_r^{\rm peak} = -14.6 \pm 0.5$; Stritzinger et al. 2014), and SN 2008 ha ($M_{\rm g}^{\rm peak} = -13.89 \pm 0.14$, $M_r^{\rm peak} = -14.25 \pm 0.14$; Valenti et al. 2009). SN 2021fcg is more than a magnitude fainter than these SNe (see Figure 5).

We note that extinction from the host galaxy can increase our estimate of the peak brightness. In the absence of any host extinction indicators (Section 2.2), we use the $(g-r)$ color of SN 2021fcg to examine the effect of host extinction on our measurements. The $(g-r)$ color of SN 2021fcg at the *r*-band peak corrected for Galactic extinction is $0.60 \pm 0.29$ mag. The corresponding value for SN 2008 ha is $0.57 \pm 0.03$ mag, for SN 2019gsc is $0.42 \pm 0.12$ mag, and for SN 2010ae is $0.42 \pm 0.04$ mag (Foley et al. 2009; Stritzinger et al. 2014; Srivastav et al. 2020). SN 2008 ha and SN 2019gsc had no significant host extinction, while $E(B-V)_{\rm host} = 0.3$ is the most appropriate value for SN 2010ae (Stritzinger et al. 2014; Srivastav et al. 2020). If SN 2021fcg has similar peak colors as the other low-luminosity SNe, the host extinction is $E(B-V)_{\rm host} \approx 0.2^{+0.3}_{-0.2}$. Using $E(B-V)_{\rm host} = 0.2$ gives $M_{r,\rm peak} = -13.16 \pm 0.20$. Even with the $E(B-V) = 0.5$, SN 2021fcg has $M_{r,\rm peak} = -13.78 \pm 0.20$ and is still among the lowest-luminosity thermonuclear supernova discovered to date. However, no relation between SN Iax peak colors has been established, so these extinction estimates are representative at best.

The right panel of Figure 2 shows the *r*-band photometric evolution of SN 2021fcg compared to other low-luminosity SN Iax. The overall evolution of SN 2021 fcg is broadly consistent, albeit slightly slower than the other three SNe. However, the slow apparent evolution might be an effect of the epoch of peak brightness not being constrained accurately. We note that the *r*- and *i*-band lightcurve flattened between +9 days and +22 days, a behavior that is not seen for the other three SNe (Figure 2). From +25 days to +80 days, the *r*-band lightcurve declined at a rate of $\approx$0.04 mag day$^{-1}$.

### 3.1. Bolometric Luminosity

We fit the photometric measurements with a blackbody function to derive the bolometric luminosity of the supernova. As our lightcurve sampling is sparse, we do not have contemporaneous multiband observations. We interpolate between the *r*- and *i*-band detections using a Gaussian process with a radial basis function kernel to generate synthetic measurements wherever necessary. The Gaussian process model was implemented using `scikit-learn`.[16] We then fit a blackbody function to these measurements with a Markov Chain Monte Carlo analysis using the `python` package `emcee` (Foreman-Mackey et al. 2013) to derive the effective temperatures, photospheric radii, and bolometric luminosities. We note that the systematic uncertainties on our estimates are large as they are derived using data for only two filters. Additionally, we do not have any ultraviolet (UV) or near-infrared (NIR) photometric coverage. For SN2019gsc, Srivastav et al. (2020) estimated that the UV and NIR contribution increases the optical blackbody luminosity by a factor of $\approx$1.5. Assuming a similar contribution for SN 2021fcg, we add a 50% systematic uncertainty to our luminosity estimates. We note that the late-time spectra do not resemble a blackbody. However, we use simple blackbody estimates as the data available is limited.

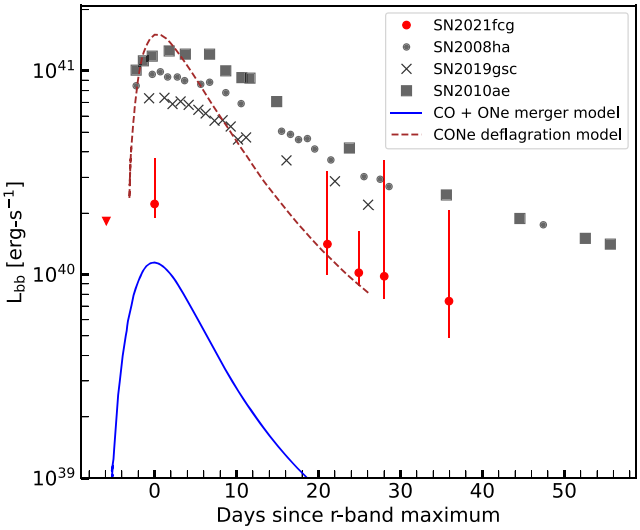


**Figure 3.** Bolometric luminosity evolution (derived from blackbody fitting) of SN 2021fcg compared with the blackbody luminosities of SNe 2008 ha, 2010ae, and 2019gsc (Srivastav et al. 2020). The peak luminosity of SN 2021fcg is smaller than the other low-luminosity SN Iax by a factor of $\sim$3. Also plotted are the theoretical bolometric luminosities of explosions from deflagration of a near-$M_{\rm ch}$ white dwarf (dashed brown line; Kromer et al. 2015) and the merger of a 1.1 $M_\odot$ CO and a 1.2 $M_\odot$ ONe white dwarf (solid blue line; Kashyap et al. 2018).

Figure 3 shows the evolution of the bolometric luminosity of SN 2021fcg compared to SN 2008 ha, SN 2010ae, and SN 2019gsc (taken from Srivastav et al. 2020). The peak bolometric luminosity is $2.5^{+1.5}_{-0.3} \times 10^{40}$ erg s$^{-1}$ which is $\sim$3 times lower than SN 2019gsc. We model the bolometric luminosity evolution using the relations from Arnett (1982) formulated as in Valenti et al. (2008). This model assumes that the lightcurve is powered by radioactive decay of $^{56}$Ni and $^{56}$Co in the ejecta. The ejecta are assumed to be spherically symmetric, homologously expanding, and have constant opacity (see Valenti et al. 2008 for additional details). Under these assumptions, the evolution of the bolometric luminosity can be described using three parameters—the total nickel mass $M_{\rm Ni}$, the lightcurve timescale ($\tau_M$), and the explosion time ($\tau_{\rm exp}$). We use `emcee` to estimate the best-fit parameters for SN 2021fcg. We derive a nickel mass of $M_{\rm Ni} = 0.8^{+0.4}_{-0.5} \times 10^{-3}\ M_\odot$. This is lower than the nickel mass in SN 2019gsc ($1.4$–$2.4 \times 10^{-3}\ M_\odot$), SN 2008 ha ($3 \times 10^{-3}\ M_\odot$), and SN 2010ae ($3$–$4 \times 10^{-3} M_\odot$) (derived in Srivastav et al. 2020).

The total ejecta mass ($M_{\rm ej}$) can be derived using the relation $M_{\rm ej} = \frac{1}{2}\tau^2_M \frac{\beta c v_{\rm peak}}{k_{\rm opt}}$ (Valenti et al. 2008), where $\beta = 13.8$, $c$ is the speed of light, $v_{\rm peak}$ is the peak photospheric velocity, and $k_{\rm opt}$ is the net opacity. We cannot estimate $v_{\rm peak}$ for SN 2021fcg as

[16] https://scikit-learn.org/stable/modules/gaussian_process.html

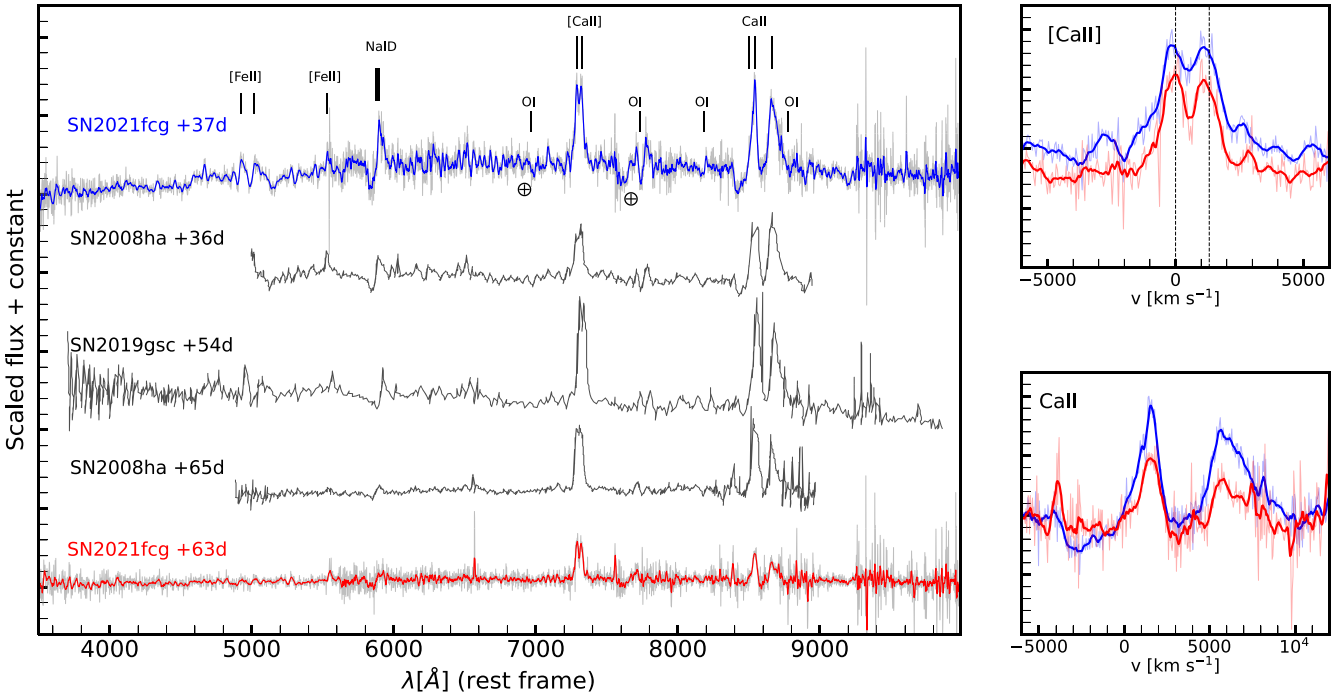


**Figure 4.** Left: late-time optical spectra of SN 2021fcg at +37 days (blue) and +63 days (red). Also plotted are similar phase spectra of SN 2008 ha and SN 2019gsc (gray; taken from Valenti et al. 2009; Tomasella et al. 2020). The spectra of SN 2021fcg closely resemble the spectra of the other low-luminosity SN Iax. Right: zoom-in of the [Ca II] (top) and Ca II (bottom) emission lines. These are the strongest features in the spectra (37 days: blue, 63 days: red). In both spectra, the peak wavelengths of [Ca II] emission are blueshifted from the rest wavelengths (black dashed lines in the top panel) by ≈100 km s$^{-1}$. The optical spectra of SN 2021fcg are available as the data behind the figure.

(The data used to create this figure are available.)

we do not have spectroscopic coverage near maximum light. We assume $v_{\rm peak} = 3500\,{\rm km\,s^{-1}}$ and $k_{\rm opt} = 0.1\ {\rm cm^2 g^{-1}}$ similar to SN 2019gsc (Srivastav et al. 2020); we derive $M_{\rm ej} = 0.05$–$0.4\ M_{\odot}$.

Finally, we note that for $E(B-V) = 0.2$ and 0.5, respectively, the peak luminosity of SN 2021fcg is $4.3^{+2.0}_{-0.6} \times 10^{40}$ erg s$^{-1}$ and $1.1^{+3.0}_{-0.3} \times 10^{41}$ erg s$^{-1}$, respectively.

## 4. Spectroscopic Evolution

Figure 4 shows the +37 day and +63 day (rest-frame phase from peak) optical spectra of SN 2021fcg. Both spectra show characteristics of late-time SN Iax spectra and closely resemble similar phase spectra of SN 2008 ha and SN 2019gsc (Valenti et al. 2009; Tomasella et al. 2020). We do not detect any hydrogen, helium, or oxygen lines in our spectra that could be indicative of a nova. In the nebular phases, the calcium lines in SN 2021fcg have velocities of ≈1500 km s$^{-1}$—much smaller than those measured for Ca-rich SNe (≈5000 km s$^{-1}$; De et al. 2020). Overall, our spectra strongly indicate that SN 2021fcg is a low-luminosity SN Iax.

The +37 day spectrum shows a slightly reddened continuum with several emission lines. The strongest emission features are the [Ca II] doublet and Ca II NIR triplet. Both of the [Ca II] doublet lines have an FWHM of ≈1300 km s$^{-1}$ (measured using Gaussian fits). We also detect a possible absorption feature for these lines at a velocity of −3500 km s$^{-1}$ (see Figure 4). For the Ca II NIR triplet, the 8498 and 8548 Å lines are blended together, with an FWHM of 1330 km s$^{-1}$. These lines also show a P-cygni profile with the emission maximum at ∼1500 km s$^{-1}$ and the absorption minimum at −2500 km s$^{-1}$. However, the absorption is likely affected by blending from other absorption lines. For the 8662 Å line, only an emission component is detected with an FWHM of 2620 km s$^{-1}$. Similar features are also seen in the spectra of SN 2019gsc and SN 2008 ha. The spectrum also shows strong Na I D emission with a P-cygni profile, although this absorption is also affected by blending. In addition, we detect several [Fe II] emission lines. We note that the O I emission is weak and no Ni or He features are detected. The +63 day spectrum is similar, with a very weak continuum. The [Ca II] doublet is the strongest emission feature with an FWHM of ≈1000 km s$^{-1}$. The Ca II NIR triplet is also detected in emission, with an FWHM of ≈1050 km s$^{-1}$ (8498 and 8548 Å) and 1850 km s$^{-1}$ (8662 Å). Compared to the +37 day spectrum, the Na I emission is very weak.

These spectral features and FWHM velocities are similar to those seen in other low-luminosity SN Iax. We also note that in both spectra, the peak wavelengths of the [Ca II] emission lines are blueshifted by ≈100 km s$^{-1}$ with respect to the rest wavelength.

## 5. Discussion

The extremely low luminosity of SN 2021fcg makes it a remarkable member of the class of thermonuclear supernovae. In Figure 5 (left panel), we compare the peak absolute magnitude and decline rate of SN 2021fcg to other thermonuclear supernovae. While the peak absolute magnitude of SN 2021fcg is ≈1.5 mag fainter than all other supernovae, its decline rate is not extreme ($\Delta m_{15,r} = 0.7 \pm 0.3$ mag), and is similar to the other three low-luminosity SN Iax.

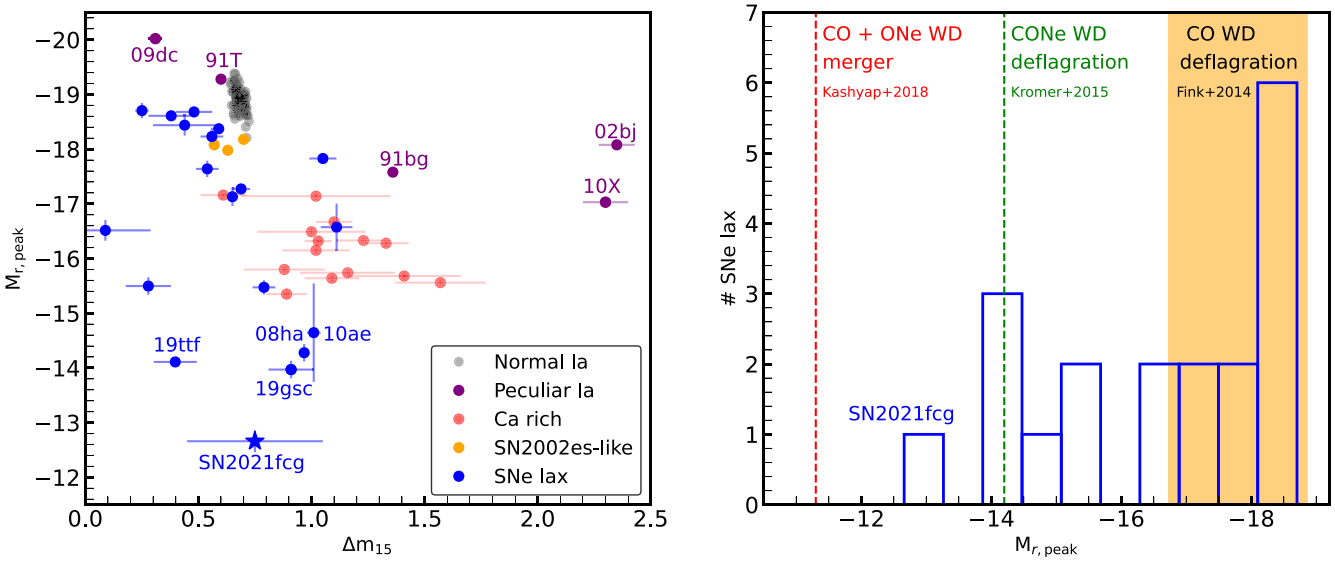


**Figure 5.** Left: peak $r$-band absolute magnitudes against $r$-band decline rates ($\Delta m_{15}$) of thermonuclear supernovae. SN 2021fcg (blue star) is the least luminous thermonuclear SN discovered to date. We also plot the values for normal SNe Ia (black circles; Yao et al. 2019); the peculiar SNe Ia 1991bg (Filippenko et al. 1992), 1991T (Lira et al. 1998), 2009dc (Taubenberger et al. 2011), 2010x (Kasliwal et al. 2010), and 2002bj (Poznanski et al. 2010) (purple circles); calcium-rich gap transients (red circles; De et al. 2020), 02es-like transients (orange circles; White et al. 2015); and SNe Iax (blue circles; Magee et al. 2016; Foley et al. 2013; Srivastav et al. 2020). We use $H_0 = 73$ km/s/Mpc to calculate the distances to all SNe, we use $H_0 = 73$ km s$^{-1}$ Mpc$^{-1}$ for all SNe. Right: a histogram of peak SN Iax absolute magnitudes together with the predictions of existing progenitor models. The bright ($M_r < -16.8$ mag) SN Iax are consistent with simulations of deflagrations of near-$M_{ch}$ CO white dwarfs (orange region; Fink et al. 2014). The lower-luminosity 08ha-like SNe are consistent with the simulation of a deflagration of hybrid CONe white dwarf (green line; Kromer et al. 2015). SN 2021fcg is even fainter, and it is unclear if it could be explained by different initial conditions of the CONe WD deflagration. A promising alternative is the double-degenerate model involving the merger of a 1.1 $M_\odot$ CO and 1.2 $M_\odot$ ONe white dwarf. A more massive ONe white dwarf could give rise to more luminous transients such as SN 2021fcg.

### 5.1. What Is the Progenitor of SN 2021fcg?

The exact origin of SN Iax is debated; however, it is generally accepted that they are associated with thermonuclear explosions of white dwarfs (Jha 2017). In particular, models involving the deflagration of a near-Chandrasekhar ($M_{ch}$) accreting white dwarf that leaves behind a bound remnant have been able to reproduce some observed properties of SN Iax. Failed deflagrations of a near-$M_{ch}$ CO white dwarf successfully explain several features of the luminous SN Iax (Jordan et al. 2012; Kromer et al. 2013; Fink et al. 2014). However, this model cannot explain the lower-luminosity 08ha-like explosions—the faintest supernova from the CO deflagration model has $M_V = -16.8$ mag (Fink et al. 2014).

Kromer et al. (2015) proposed that the low-luminosity SN Iax could be deflagrations of hybrid CONe white dwarfs (Chen et al. 2014; Denissenkov et al. 2015). The presence of the ONe layer can quench the burning to suppress the amount of nickel produced. They simulated the deflagration of a 1.4 $M_\odot$ CONe white dwarf with five ignition cores and found that this results in a low-luminosity ($M_V \approx -14.2$) transient roughly consistent with SN 08 ha, 10ae, and 19gsc. However, they derive a total ejecta mass of 0.014 $M_\odot$—an order of magnitude smaller than SN 08 ha, 10ae, and 19gsc. Consequently, the transient in their simulations evolves faster than these three SN (see Figure 3).

SN 2021fcg is fainter than the CONe deflagration model by $\approx$1.5 mag. In order to explain the luminosity and timescale of SN 2021fcg as the outcome of a white dwarf deflagration, the nickel ejecta mass has to be lower by a factor of $\sim$3 and the total ejecta mass has to be at least 10 times larger than the value obtained by Kromer et al. (2015). It remains to be seen if a lower number of ignition cores or a larger ONe mass than the one used by Kromer et al. (2015) can reduce the nickel yield enough to explain the low luminosity of SN 2021fcg. However, a lower total ejecta mass will make the transient even faster evolving and inconsistent with the slow decline rate of SN 2021fcg. SN 2021fcg is thus a challenge to the existing picture of hybrid white dwarf deflagration and warrants further investigation of this channel.

An alternative picture for formation of low-luminosity SNe Iax is the double-degenerate scenario. Kashyap et al. (2018) showed that the merger of a CO and ONe white dwarf yields a failed detonation of the ONe core producing small amounts of ejecta. This gives rise to a very faint, rapidly evolving transient. They modeled the merger of a 1.1 $M_\odot$ CO and a 1.2 $M_\odot$ ONe white dwarf and derive a very low nickel yield ($5.7 \times 10^{-4}$ $M_\odot$). The resulting transient has a peak $M_V = -11.3$, an ejecta velocity of $\sim$4000 km s$^{-1}$, and a total ejecta mass of $\sim$0.08 $M_\odot$.

The observed luminosity of SN 2021fcg is $\sim$3 times brighter than that predicted by Kashyap et al. (2018) (see Figure 3), while the nickel and total ejecta masses are roughly consistent with their estimates. The double-degenerate channel is thus a promising model to explain SN 2021fcg, as a merger involving a more massive ONe white dwarf could give a brighter and longer lived transient than the one modeled in Kashyap et al. (2018). However, the requirement of a more massive ONe white dwarf may decrease the expected rate of such explosions. Additional studies of this model are necessary to test its viability as the progenitor of SN 2021fcg. In this channel, the remnant is a kicked super-Chandrasekhar star with an ONe core embedded in the nebulosity of the SN ejecta. Recently, Oskinova et al. (2020) identified a candidate super-$M_{ch}$ remnant at the center of the nebula IRAS00500+6713. They posit that this source is the remnant of an SN Iax resulting from an ONe and CO white dwarf merger. If SN 2021fcg is the result of a white dwarf merger, the remnant would be a similar super-$M_{ch}$ star that will eventually end its life as an electron-capture SN.

In any of these scenarios, the surviving bound remnant can drive winds from its surface through delayed radioactive decay (Shen & Schwab 2017). These winds can be the dominant source of luminosity at late times (≈1 yr post-explosion) lasting for at least a decade. Recent Hubble Space Telescope (HST) observations of SN 2012Z revealed an excess in its late-time luminosity that could be a result of remnant-driven winds (McCully et al. 2021). Late-time HST observations of SN 2021fcg will be valuable in probing the nature of its bound remnant.

We summarize these possible formation scenarios in the right panel of Figure 5. Additional scenarios that do not invoke a white dwarf have also been proposed to explain other low-luminosity SNe Iax. For example, Valenti et al. (2009) note that SN 2008 ha has similarities with models of low-luminosity core-collapse SN such as a fallback massive star SN (Moriya et al. 2010) or an ultra-stripped electron-capture SN (Pumo et al. 2009). NIR spectra can help distinguish between a thermonuclear and core-collapse origin for these supernovae (Stritzinger et al. 2015).

## 6. Conclusions

We have presented optical photometry and late-time optical spectroscopy for SN 2021fcg—the faintest SN-like transient discovered to date. The photometric and spectroscopic evolution of SN 2021fcg closely resembles faint SN Iax such as SN 2008 ha, SN 2010ae, and SN 2019gsc. SN 2021fcg has $M_r = -12.66 \pm 0.20$ mag and is the faintest of the faint SN Iax, fainter than the other members by more than a magnitude. The lower luminosity, lower nickel ejecta mass, and slightly slower photometric evolution of SN 2021fcg represent a challenge to theoretical models of faint SN Iax. Existing hybrid CONe white dwarfs deflagration models are overluminous by a factor of ∼3. A double-degenerate scenario in which the SN is an outcome of a CO and ONe white dwarf merger is a promising model. Formation channels that involve a core-collapse origin are also plausible, but unlikely.

Additional observations of SN Iax with extremely low luminosities ($M \approx -12.5$ mag) are required to identify the explosion mechanisms of these mysterious transients. ZTF can detect these SNe to a distance of ≈40 Mpc. The Vera Rubin Observatory (VRO; Ivezić et al. 2019) will significantly increase the discovery distance to ≈275 Mpc. However, given the fast evolution of these transients, rapid follow-up observations will be required to derive useful insights about them. An experiment similar to the Census of the Local Universe (De et al. 2020) that keeps track of VRO transients in cataloged galaxies will be instrumental in discovering such low-luminosity SNe.

We thank the anonymous reviewer for comments that helped improve the paper. We thank Harsh Kumar, Varun Bhalerao, and G. C. Anupama for photometric observations with the GROWTH-India telescope (https://sites.google.com/view/growthindia/). This Letter is based on observations obtained with the Samuel Oschin Telescope 48 inch and the 60 inch Telescope at the Palomar Observatory as part of the Zwicky Transient Facility project. ZTF is supported by the National Science Foundation under grant No. AST-2034437 and a collaboration including Caltech, IPAC, the Weizmann Institute for Science, the Oskar Klein Center at Stockholm University, the University of Maryland, Deutsches Elektronen-Synchrotron and Humboldt University, the TANGO Consortium of Taiwan, the University of Wisconsin at Milwaukee, Trinity College Dublin, Lawrence Livermore National Laboratories, and IN2P3, France. Operations are conducted by COO, IPAC, and UW. SED Machine is based upon work supported by the National Science Foundation under grant No. 1106171. This work is also based on observations made with the Nordic Optical Telescope, owned in collaboration by the University of Turku and Aarhus University, and operated jointly by Aarhus University, the University of Turku and the University of Oslo, representing Denmark, Finland and Norway, the University of Iceland and Stockholm University at the Observatorio del Roque de los Muchachos, La Palma, Spain, of the Instituto de Astrofisica de Canarias. SED Machine is based upon work supported by the National Science Foundation under grant No. 1106171. The ZTF forced photometry service was funded under the Heising-Simons Foundation grant 12540303 (PI: Graham). K.M. is funded by the EU H2020 ERC grant No. 758638. S.S. and E.C.K. acknowledge support from the G.R.E. A.T research environment, funded by *Vetenskapsrådet*, the Swedish Research Council, project number 2016-06012. E.C. K. acknowledges support from The Wenner-Gren Foundations. M.R. has received funding from the European Research Council (ERC) under the European Union's Horizon 2020 research and innovation program (grant agreement 759194—USNAC).

## ORCID iDs

Viraj R. Karambelkar https://orcid.org/0000-0003-2758-159X
Mansi M. Kasliwal https://orcid.org/0000-0002-5619-4938
Kate Maguire https://orcid.org/0000-0002-9770-3508
Shreya G. Anand https://orcid.org/0000-0003-3768-7515
Igor Andreoni https://orcid.org/0000-0002-8977-1498
Dmitry A. Duev https://orcid.org/0000-0001-5060-8733
Matthew J. Graham https://orcid.org/0000-0002-3168-0139
Erik C. Kool https://orcid.org/0000-0002-7252-3877
Russ R. Laher https://orcid.org/0000-0003-2451-5482
Mark R. Magee https://orcid.org/0000-0002-0629-8931
Ashish A. Mahabal https://orcid.org/0000-0003-2242-0244
Michael S. Medford https://orcid.org/0000-0002-7226-0659
Daniel Perley https://orcid.org/0000-0001-8472-1996
Mickael Rigault https://orcid.org/0000-0002-8121-2560
Ben Rusholme https://orcid.org/0000-0001-7648-4142
Steve Schulze https://orcid.org/0000-0001-6797-1889
Yashvi Sharma https://orcid.org/0000-0003-4531-1745
Jesper Sollerman https://orcid.org/0000-0003-1546-6615
Yuhan Yao https://orcid.org/0000-0001-6747-8509

## References

Arnett, W. D. 1982, ApJ, 253, 785
Bellm, E. C., Kulkarni, S. R., Graham, M. J., et al. 2019, PASP, 131, 018002
Blagorodnova, N., Neill, J. D., Walters, R., et al. 2018, PASP, 130, 035003
Chen, M. C., Herwig, F., Denissenkov, P. A., & Paxton, B. 2014, MNRAS, 440, 1274
De, K., Kasliwal, M. M., Tzanidakis, A., et al. 2020, ApJ, 905, 58
Dekany, R., Smith, R. M., Riddle, R., et al. 2020, PASP, 132, 038001
Denissenkov, P. A., Truran, J. W., Herwig, F., et al. 2015, MNRAS, 447, 2696
Duev, D. A., Mahabal, A., Masci, F. J., et al. 2019, MNRAS, 489, 3582
Filippenko, A. V., Richmond, M. W., Branch, D., et al. 1992, AJ, 104, 1543
Fink, M., Kromer, M., Seitenzahl, I. R., et al. 2014, MNRAS, 438, 1762
Foley, R. J., Challis, P. J., Chornock, R., et al. 2013, ApJ, 767, 57
Foley, R. J., Chornock, R., Filippenko, A. V., et al. 2009, AJ, 138, 376
Foreman-Mackey, D., Hogg, D. W., Lang, D., & Goodman, J. 2013, PASP, 125, 306

Graham, M. J., Kulkarni, S. R., Bellm, E. C., et al. 2019, PASP, 131, 078001
Ivezić, Ž., Kahn, S. M., Tyson, J. A., et al. 2019, ApJ, 873, 111
Jha, S. W. 2017, in Handbook of Supernovae, ed. A. W. Alsabti & P. Murdin (Zurich: Springer), 375
Jordan, G. C. I., Perets, H. B., Fisher, R. T., & van Rossum, D. R. 2012, ApJL, 761, L23
Kashyap, R., Haque, T., Lorén-Aguilar, P., García-Berro, E., & Fisher, R. 2018, ApJ, 869, 140
Kasliwal, M. M., Cannella, C., Bagdasaryan, A., et al. 2019, PASP, 131, 038003
Kasliwal, M. M., Kulkarni, S. R., Gal-Yam, A., et al. 2010, ApJL, 723, L98
Kourkchi, E., & Tully, R. B. 2017, ApJ, 843, 16
Kromer, M., Fink, M., Stanishev, V., et al. 2013, MNRAS, 429, 2287
Kromer, M., Ohlmann, S. T., Pakmor, R., et al. 2015, MNRAS, 450, 3045
Li, W., Filippenko, A. V., Chornock, R., et al. 2003, PASP, 115, 453
Lira, P., Suntzeff, N. B., Phillips, M. M., et al. 1998, AJ, 115, 234
Magee, M. R., Kotak, R., Sim, S. A., et al. 2016, A&A, 589, A89
Masci, F. J., Laher, R. R., Rusholme, B., et al. 2019, PASP, 131, 018003
McCully, C., Jha, S. W., Foley, R. J., et al. 2014, Natur, 512, 54
McCully, C., Jha, S. W., Scalzo, R. A., et al. 2021, arXiv:2106.04602
Moriya, T., Tominaga, N., Tanaka, M., et al. 2010, in AIP Conf. Ser. 1279, Deciphering the Ancient Universe with Gamma-ray Bursts, ed. N. Kawai & S. Nagataki (New York: AIP), 224
Mould, J. R., Huchra, J. P., Freedman, W. L., et al. 2000, ApJ, 529, 786
Oke, J. B., Cohen, J. G., Carr, M., et al. 1995, PASP, 107, 375
Oskinova, L. M., Gvaramadze, V. V., Gräfener, G., Langer, N., & Todt, H. 2020, A&A, 644, L8
Patterson, M. T., Bellm, E. C., Rusholme, B., et al. 2019, PASP, 131, 018001
Perley, D. A. 2019, PASP, 131, 084503
Poznanski, D., Chornock, R., Nugent, P. E., et al. 2010, Sci, 327, 58
Pumo, M. L., Turatto, M., Botticella, M. T., et al. 2009, ApJL, 705, L138
Rigault, M., Neill, J. D., Blagorodnova, N., et al. 2019, A&A, 627, A115
Schlafly, E. F., & Finkbeiner, D. P. 2011, ApJ, 737, 103
Shen, K. J., & Schwab, J. 2017, ApJ, 834, 180
Smith, K. W., Smartt, S. J., Young, D. R., et al. 2020, PASP, 132, 085002
Srivastav, S., Smartt, S. J., Leloudas, G., et al. 2020, ApJL, 892, L24
Stritzinger, M. D., Hsiao, E., Valenti, S., et al. 2014, A&A, 561, A146
Stritzinger, M. D., Valenti, S., Hoeflich, P., et al. 2015, A&A, 573, A2
Taubenberger, S., Benetti, S., Childress, M., et al. 2011, MNRAS, 412, 2735
Theureau, G., Hanski, M. O., Coudreau, N., Hallet, N., & Martin, J.-M. 2007, A&A, 465, 71
Tomasella, L., Stritzinger, M., Benetti, S., et al. 2020, MNRAS, 496, 1132
Tonry, J. L., Denneau, L., Heinze, A. N., et al. 2018, PASP, 130, 064505
Valenti, S., Benetti, S., Cappellaro, E., et al. 2008, MNRAS, 383, 1485
Valenti, S., Pastorello, A., Cappellaro, E., et al. 2009, Natur, 459, 674
van der Walt, S. J., Crellin-Quick, A., & Bloom, J. S. 2019, JOSS, 4, 1247
White, C. J., Kasliwal, M. M., Nugent, P. E., et al. 2015, ApJ, 799, 52
Yao, Y., Miller, A. A., Kulkarni, S. R., et al. 2019, ApJ, 886, 152
Zackay, B., Ofek, E. O., & Gal-Yam, A. 2016, ApJ, 830, 27